# Neutron-capture cross sections for osmium isotopes and the age of the universe

J. C. Browne* and B. L. Berman
*Lawrence Livermore Laboratory, University of California, Livermore, California 94550*
(Received 25 August 1980)

The neutron-capture cross sections for $^{186,187,188,189,190,192}$Os have been measured by the neutron-time-of-flight technique from 0.5 eV to 150 keV. Nuclear level spacings were extracted from the low-energy (resonance-region) data below ~1 keV, and average cross sections from the data above 1 keV. The ratio of the Maxwellian-weighted average cross sections for $^{186}$Os and $^{187}$Os near 30 keV is a vital parameter for the determination of the duration of nucleosynthesis prior to the formation of the solar system, and thus for the determination of the age of the universe by the nuclear-dating technique. The present result of $10.8^{+1.4}_{-2.2}\times10^9$ yr for the duration of nucleosynthesis is in concordance with the value obtained from U-Th dating. The result for the age of the universe ($17\pm3\times10^9$ yr) agrees with the value obtained from the globular-cluster method, but clearly exceeds the most recent determination of the Hubble time.

[NUCLEAR REACTIONS $^{186,187,188,189,190,192}$Os$(n,\gamma)$, $E=2$–$1.5\times10^5$ eV; measured $\sigma(n,\gamma)$; Maxwellian-averaged $\sigma(kT=30$ keV); extracted average level spacing; deduced age of universe for Re-Os clock.]

## I. INTRODUCTION

Because the half-life of $^{187}$Re is very long ($\sim43\times10^9$ yr), because both $^{186}$Os and $^{187}$Os are pure $s$-process nuclei (i.e., they are shielded by $^{186}$W and $^{187}$Re, respectively, from the $r$-process), and because these heavy metals are present in a relatively undisturbed state in primordial meteorites, the $^{187}\text{Re}\rightarrow{}^{187}$Os nuclear $\beta$-decay clock constitutes probably the best basis for a radiogenic determination of the age of the elements. This method was suggested originally by Clayton,[1] who pointed out its advantages, particularly over those methods that depend upon a knowledge of the $r$-process production rates.

Clayton also pointed out the key role played by the neutron-capture cross sections for $^{186}$Os and $^{187}$Os (or rather, by their ratio) in this determination. Such measurements, however, would have been beset with formidable experimental difficulties until the sufficiently massive and isotopically pure samples of these rare osmium isotopes were manufactured for the measurements reported here.[2] Subsequent measurements using these enriched samples have been reported by Browne *et al.*[3] and by Winters *et al.*[4] The results of all three measurements are compared in Sec. IV.

In addition to the required ratio of Maxwellian-averaged 30-keV cross sections, a correction factor is needed in order to account for neutron capture by $^{187}$Os nuclei in their 9.8-keV first excited state, which also is populated significantly in a stellar environment. A Hauser-Feshbach calculation[5] of this correction factor has been made by Woosley and Fowler.[6] Among the important input parameters for this calculation are the average level spacings for $^{187}$Os ($^{186}\text{Os}+n$) and $^{188}$Os ($^{187}\text{Os}+n$). We have been able to extract improved values for these level spacings as well from our low-energy (<1 keV) data.

These results, together with values for the half-life of $^{187}$Re and the elemental abundance ratio of osmium and rhenium in carbonaceous chrondites and the use of an exponential model of the supernova rate ($r$-process nucleosynthesis) in our galaxy, enable one to obtain the time duration of nucleosynthesis $\Delta$ prior to the formation of the solar system. This value for $\Delta$, when added to the known age of the solar system ($4.7\times10^9$ yr), then yields the age of the galaxy (the age of the elements). Adding another 1 to $2\times10^9$ yr for galaxy formation (from the time of the big bang) yields in turn the age of the universe. Our results for the age of the universe are compared in Sec. V with those based upon other methods, and their cosmological implications are noted.

## II. EXPERIMENTAL PROCEDURE

This experiment was performed at the neutron time-of-flight (TOF) facility at the Lawrence Livermore Laboratory Electron-Positron Linear Accelerator. A schematic diagram of the experimental arrangement is shown in Fig. 1. Neutrons were produced in a water-cooled tantalum target struck by a 115-MeV electron beam. The linac was pulsed at 600 Hz with a pulse width of 11 ns. The energy of the neutrons was determined by their times of flight down an evacuated, collimated flight tube to the samples located 14.7 m from the neutron source. The collimation consisted of a series of brass, borated polyethylene, lead, and bismuth collimators. After the neutron

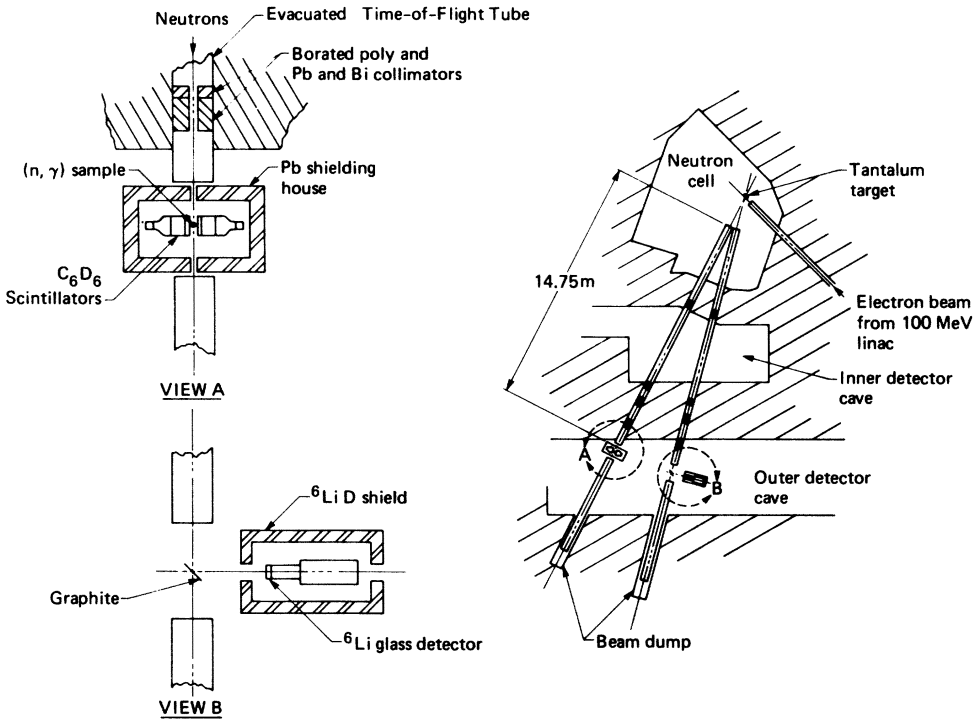


FIG. 1. Schematic diagram of the experimental arrangement. The samples were located between two $C_6D_6$ scintillators. The neutron flux was monitored on a separate flight path using a $^6$Li glass scintillator.

beam passed through the samples, it proceeded 3 m into a get-lost pipe in concrete shielding. The shape of the neutron flux was determined by scattering the neutrons from a thin graphite foil into a $^6$Li glass detector (NE905). This detector was located on an adjacent flight path, as shown in Fig. 1. A measurement of the flux shape for both flight paths was performed in a separate experiment using the same detector setup. When the background-subtracted data for the flux measurements on the two flight paths were overlayed on the same energy scale and were normalized to the same total neutron flux, there were no discernible differences in the shape of the flux within the statistical accuracy of the measurements (2–3 % depending upon energy range and channel width). This detector also served as a neutron monitor for cycling the capture samples, as discussed below.

The measurement was performed with samples of enriched $^{186}$Os, $^{187}$Os, $^{188}$Os, $^{189}$Os, $^{190}$Os, and $^{192}$Os in the form of metallic powder. In addition, samples of natural osmium, carbon, and $^{165}$Ho were included. The natural osmium sample also was metallic powder; the carbon sample was graphite powder; and the $^{165}$Ho was an oxide sample. Each sample was enclosed in a light-weight beryllium container in order to minimize neutron capture in the sample containers. An empty container also was included in the measurement. Therefore, a total of ten samples was involved in the measurement. The relative isotopic abundances of the osmium samples are listed in Table I. The mass and thickness of each sample is listed in Table II. The ten samples were attached to a thin but inflexible string which ran through a pulley arrangement driven by a computer-controlled stepping motor. The position and identification of each sample was determined via holes in an inflexible Mylar-based paper tape which passed through a light-emitting diode (LED) encoder. After a preset scalar reached a given number of preset neutron-flux monitor counts, a computer (PDP-8/I) stopped the data acquisition, cycled the stepping motor to the next sample as determined by the LED encoder, printed out the readings from a series of scalars related to that cycle, and then restarted the data collection. Each sample was in the neutron beam for approximately ten minutes before cycling to the next sample. The total amount of time that a given sample was in the neutron beam was dependent upon its overall count rate. This cycling was an attempt to smooth out any short-term variations in the beam and to achieve similar counting statistics for each osmium sample.

TABLE I. Relative isotopic abundances of the osmium samples.

| Sample | Isotopic abundance (atom-%) | | | | | | |
|---|---|---|---|---|---|---|---|
| | $^{184}$Os | $^{186}$Os | $^{187}$Os | $^{188}$Os | $^{189}$Os | $^{190}$Os | $^{192}$Os |
| $^{186}$Os | <0.02 | 78.39 | 1.62 | 5.07 | 4.09 | 5.15 | 5.67 |
| $^{187}$Os | <0.05 | 0.88 | 70.96 | 12.58 | 5.09 | 5.31 | 5.17 |
| $^{188}$Os | <0.05 | <0.05 | <0.10 | 94.41 | 3.26 | 1.28 | 1.04 |
| $^{189}$Os | 0.04 | 0.05 | 0.06 | 0.80 | 95.40 | 2.61 | 1.04 |
| $^{190}$Os | <0.005 | <0.03 | 0.015 | 0.26 | 0.61 | 98.14 | 0.97 |
| $^{192}$Os | <0.02 | 0.04 | 0.06 | 0.13 | 0.22 | 0.47 | 99.07 |
| $^{nat}$Os | 0.02 | 1.6 | 1.6 | 13.3 | 16.1 | 26.4 | 41.0 |

Capture $\gamma$ rays were detected by a pair of deuterated benzene ($C_6D_6$) liquid scintillators (one liter each) arranged as shown in Fig. 1 in order to subtend a sizable fraction of a $4\pi$ solid angle. The $\gamma$-ray bias level was adjusted to exclude events for which the energy deposited was less than that of Compton electrons from 300-keV $\gamma$ rays. The response function was measured for these conditions using a set of eight radioactive sources covering the $\gamma$-ray energy range from 356 keV ($^{133}$Ba) to 2.615 MeV ($^{228}$Th). The response for $C_6D_6$ above this energy range was determined from the previous measurements of Czirr.[7]

Both the neutron time of flight and the pulse height for each capture event were stored on a magnetic drum in a two-dimensional (2D) array consisting of 64 pulse-height channels by 6000 time-of-flight (TOF) channels for each sample. A similar (2D) array was accumulated for the $^6$Li flux detector. A cadmium filter was present in each TOF path to eliminate pulse-to-pulse overlap. Details of the electronic setup are discussed in Ref. 8. The computer data acquisition system is described in Ref. 9.

## III. DATA ANALYSIS

### A. Capture data

The two-dimensional (2D) ($\gamma$-ray pulse height vs neutron time of flight) data for each sample were reduced to two TOF spectra. A weighted TOF spectrum was obtained by weighting the $\gamma$-ray pulse height according to the measured response function of the $C_6D_6$ detectors. The weighted yield $Y_i(t_i)$ for a given time of flight $t_i$ is

$$Y_i(t_i) = \sum_j w_j Y_{ij}(t_i) ,$$

where $w_j$ is the weighting factor for pulse height $j$ and $Y_{ij}$ is the number of counts for pulse height $j$. This is the Maier-Leibnitz technique,[10] which results in the efficiency of the $\gamma$-ray detectors being made independent of the capture $\gamma$-ray cascade spectrum. The response function for $C_6D_6$ has been discussed by Czirr.[7] An unweighted TOF spectrum was obtained simply by summing all the pulse-height data for a given time of flight. The weighted TOF spectrum was corrected for dead-time effects using the unweighted TOF spectrum for a fixed 8-$\mu$s dead time appropriate for the conditions of the experiment. A TOF spectrum for $^{187}$Os + $n$ below 1 keV neutron energy is shown in Fig. 2.

TABLE II. Sample masses and thicknesses.

| Sample | Mass (g) | Thickness (atoms/b) |
|---|---|---|
| $^{186}$Os | 3.278 | $4.1\times10^{-3}$ |
| $^{187}$Os | 2.959 | $3.5\times10^{-3}$ |
| $^{188}$Os | 2.142 | $2.9\times10^{-3}$ |
| $^{189}$Os | 2.354 | $3.8\times10^{-3}$ |
| $^{190}$Os | 2.247 | $1.1\times10^{-2}$ |
| $^{192}$Os | 2.215 | $4.3\times10^{-3}$ |
| $^{nat}$Os | 2.332 | $3.3\times10^{-3}$ |
| $Ho_2O_3$ | 2.245 | $3.4\times10^{-3}$ |
| C | 0.473 | $1.0\times10^{-2}$ |

The data rates for this measurement were much less than one event per linac beam burst, so that the dead-time corrections were small (<2%). The background was measured using both a blank sample (an empty beryllium sample container) and a carbon sample to simulate the neutron scattering cross sections of the osmium samples. The blank-sample background consisted of both accelerator-dependent and -independent effects. The sum of these effects was quite large relative to the true counting rates for the even isotope samples (~60 to 70%), but was consistent from cycle to cycle (<2% variation). The neutron-scattering background determined from the carbon sample was much smaller, varying between 4% and 7%, depending upon the sample. The uncertainties in the cross sections resulting from these background corrections was less than 2% for the odd osmium isotopes and reached 15% for the even isotopes.

The data also were corrected for the effect of

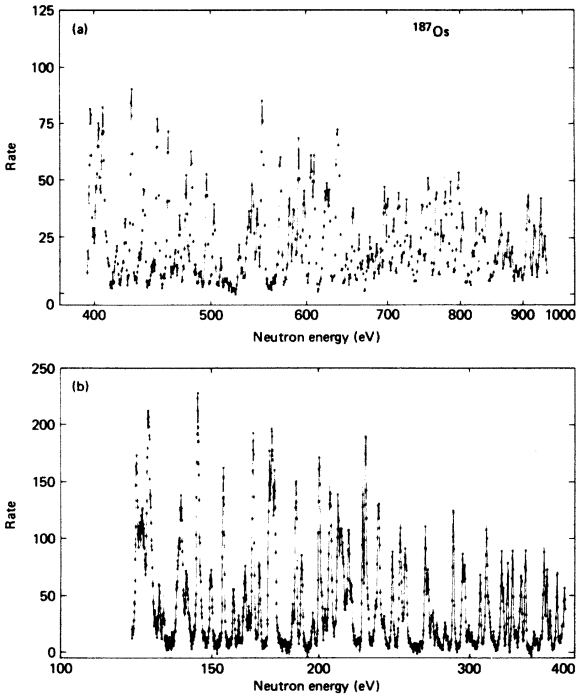


FIG. 2. A plot of the $^{187}$Os$(n, \gamma)$ capture yield from 125 to 950 eV neutron energy. The background has been subtracted from the data (as can be seen from the offset zero).

$\gamma$-ray absorption in the sample, assuming a typical capture spectrum. This resulted in a 5 to 6% correction to the capture yield, and was only slightly dependent upon the sample species.

Since a given sample contained significant impurities of the other osmium isotopes, a correction to the observed capture yield was made in order to account for this effect. The observed yield $Y_i^{\text{obs}}$ for a given isotope $i$ can be written as

$$Y_i^{\text{obs}}(E) = Y_i^0(E) + \sum_j Y_j(E) ,$$

where $Y_i^0$ is the yield from the isotope of interest and $Y_j$ is the yield from the impurity isotope $j$. The quantity $Y_j$ can be written as $C_{ij} Y_j^0$, where $Y_j^0$ is the yield for a 100% pure sample of isotope $j$ and $C_{ij}$ is the normalization for the impurity $j$ which depends upon its concentration in sample $i$ (Table I). The purity is highest for $^{192}$Os and generally decreases as one goes lower in mass. Therefore, an iterative procedure was chosen which replaces $Y_j^0$ with $Y_j^{\text{obs}}$ for the first iteration. The corrections were done in order of decreasing atomic weight. After two iterations the change was less than 0.5%.

Corrections to the data were made for effects of the sample thicknesses (listed in Table II). Below 30 keV, the main effect was resonance self-shielding. For the even osmium isotopes, the correction was 10 to 15% near 2 to 3 keV except for $^{190}$Os, for which the correction was ~25%. For $^{187}$Os and $^{189}$Os, the corrections for resonance self-shielding were ~6% near 3 keV. Multiple-scattering corrections were calculated using a method similar to that described by Dresner.[11] These corrections were smaller than resonance self-shielding below 30 to 40 keV. The multiple-scattering correction varied from 1 to 2% near 30 keV to ~ 3 to 4% near 100 keV, depending upon the sample.

### B. Flux data

The 2D data obtained for the $^6$Li glass detector were converted to a neutron TOF spectrum simply by setting a lower-level bias after examining the pulse-height information at various incident neutron energies. Since the flux was determined by detecting neutrons scattered at 90° from the graphite foil, it was necessary to make corrections to the data to account for the energy loss in the scattering process. The efficiency of the $^6$Li detector was obtained using the $^6$Li$(n, \alpha)$ cross section from the ENDF/B-IV evaluated file[12] up to 150 keV. In addition, it was necessary to correct the efficiency of the $^6$Li glass detector for the other constituents in the glass (Ce, Al, O, Si, and Mg). This was done using the results of the Monte Carlo study by Zetterström, Schwarz, and Strömberg[13] of the potential and resonance scattering corrections to the efficiency of a 3.8 cm diam by 0.95 cm thick $^6$Li glass detector which is identical in size and geometry to the one employed in this measurement. The background for the $^6$Li glass detector was measured using the "black-resonance" technique. The resonance filters (and energies) were Au (4.96 eV), Mn (337 eV), Bi (800 eV and 2.3 keV), Fe (26.6 keV), and Mg (83 keV). The background in the flux data varied from 12% at 100 keV to 20% at 1 keV. Subtraction of this background gives rise to less than 4% uncertainty in the absolute cross-section scale and does not affect the ratio of any two cross sections at all.

### C. Conversion of the yield data to cross sections

The capture yields were converted to cross sections using the "saturated-resonance" technique.[14] For this measurement, the 3.92-eV resonance of $^{165}$Ho was chosen because its neutron width ($\Gamma_n = 2.4$ meV) is much smaller than its capture width ($\Gamma_\gamma = 85$ meV). This means that virtually all neutrons whose energies lie near the peak of the resonance are captured. From the measured capture yield and the flux yield, one can calculate the

overall $\gamma$-ray detection efficiency normalization $\eta$ to be

$$\eta = \frac{Y_\gamma(3.92\text{ eV})\epsilon_n(3.92\text{ eV})}{Y_n(3.92\text{ eV})\epsilon_\gamma[B_n(\text{Ho})]},$$

where $Y_\gamma$ is the resonance peak capture yield near 3.92 eV, $Y_n$ is the $^6$Li-glass-detector neutron yield, $\epsilon_n$ is the $^6$Li-glass-detector efficiency, and $\epsilon_\gamma$ is the relative efficiency for the $C_6D_6$ detector, which is dependent upon the neutron binding energy $B_n$ for $^{165}$Ho. From this, the capture cross section $\sigma_c^A$ for a given isotope $A$ can be calculated as

$$\sigma_c^A(E_n) = \frac{1}{N_A \epsilon_\gamma^A(E_n)} \frac{Y_\gamma(E_n)}{Y_n(E_n)} \frac{\epsilon_n(E_n)}{\eta},$$

where $Y_\gamma$ is the capture yield at $E_n$, $Y_n$ is the $^6$Li-glass-detector neutron yield at $E_n$, $\epsilon_n(E_n)$ is the $^6$Li-glass-detector efficiency at $E_n$, $N_A$ is the number of atoms/unit area, and $\epsilon_\gamma^A = E_\gamma[B_n(A) + E_n(\text{c.m.})]$ is the $C_6D_6$ relative efficiency for the total energy release in isotope $A$.

## IV. RESULTS

### A. Level spacings

For each osmium sample a "staircase" plot, i.e., the cumulative sum of the number of resonances as a function of neutron energy, was made. These plots are shown in Figs. 3, 4, and 5. Wigner distributions for each of these level spacings are shown in Fig. 6.

The Dyson-Mehta $\Delta_3$ statistic[15] is a measure of the mean-square deviation of the staircase plot from a straight-line fit, which can indicate a long-range ordering of the level spacings if one can show that there are no missing or misassigned levels. For example, the average level spacing obtained from a fit to the distribution of Fig. 3 for

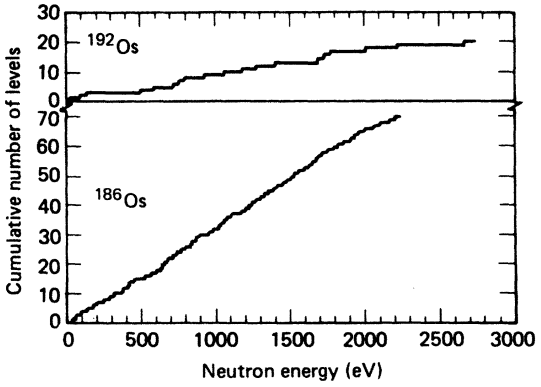


FIG. 3. A plot of the cumulative sum of levels for $^{186}$Os + $n$ and $^{192}$Os + $n$. A straight-line fit to these data yields the average level spacing $\bar{D}$, as discussed in the text.

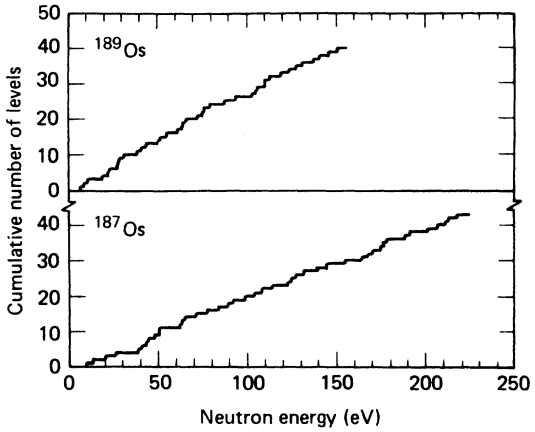


FIG. 4. A plot of the cumulative sum of levels for $^{187}$Os + $n$ and $^{189}$Os + $n$.

$^{186}$Os + $n$ is $\bar{D} = 30 \pm 2$ eV. The experimental value for $\Delta_3$ is 0.53, while the theoretical value of $\Delta_3$ for a one-spin population and the number of levels (56) in Fig. 3 for $^{186}$Os + $n$ is $0.41 \pm 0.11$. The agreement between the theoretical and experimental values of $\Delta_3$ is reasonable, indicating that there are few, if any, missed levels. This can be seen as well from the Wigner distribution for $^{186}$Os + $n$ shown in Fig. 6.

Table III lists the average level spacings $\bar{D}$ extracted from these data, along with the experimental and theoretical values of $\Delta_3$ appropriate for one-spin and two-spin populations, respectively, depending upon whether the target isotope is even or odd. Also included for comparison are the results of previous measurements.

The agreement for $\bar{D}$ between the present results for $^{187}$Os and $^{189}$Os and those of Stolovy *et al.*[16] is quite good, although the technique of Ref.

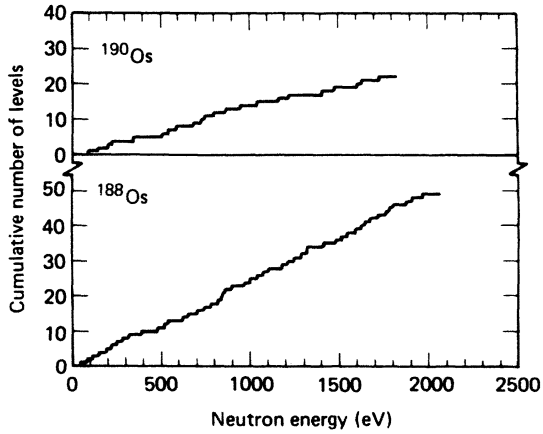


FIG. 5. A plot of the cumulative sum of levels for $^{188}$Os + $n$ and $^{190}$Os + $n$.

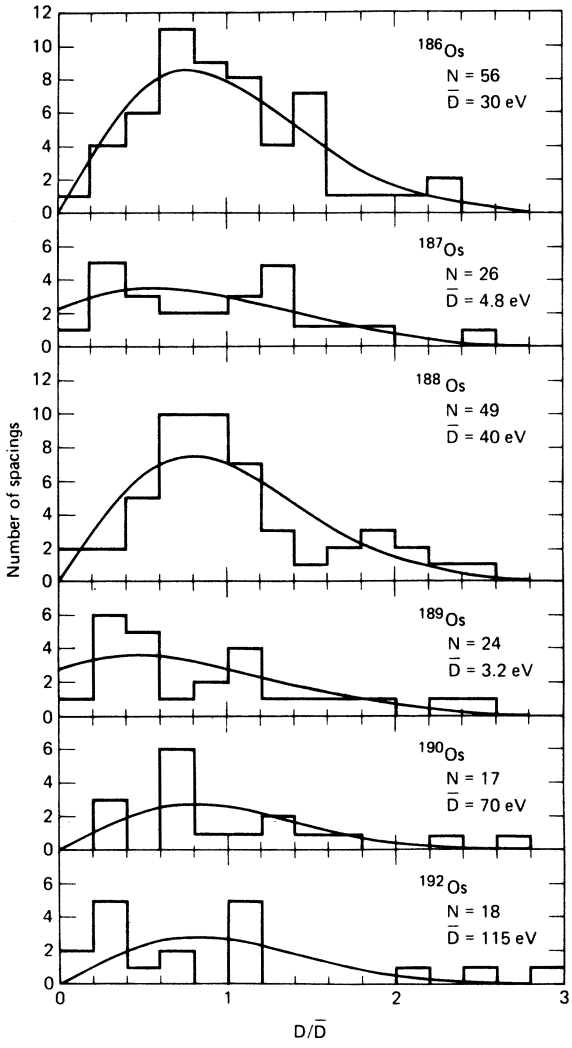


FIG. 6. Histogram of the spacings of resonances for all of the osmium isotopes studied in this experiment. The smooth curve represents the appropriate Wigner frequency function appropriate to the target spin.

16 is probably more sensitive because deexcitation $\gamma$ rays were used to assign levels to a given nucleus. The experimental values of $\Delta_3$ for these odd nuclei are in good agreement with the theoretical values of $\Delta_3$ for two-spin populations. However, the experimental values of $\Delta_3$ for the even isotopes are consistently larger than the theoretical values of $\Delta_3$ for a one-spin population. This probably means that we have missed some small levels for the even isotopes and that therefore the values of $\Delta_3$(expt) are slightly too high. This is evident as well from the Wigner distributions shown in Fig. 6.

The agreement between the present results for $\bar{D}$ and those of Ref. 17 is reasonable but not good. In particular, the values for $^{186}$Os, $^{190}$Os, and $^{192}$Os are barely within the quoted uncertainties of the two measurements, and the value given in Ref. 17 for $^{187}$Os is unreasonably large (or the quoted uncertainty is unreasonably small). The present measurement employed samples of higher purity and had a resolution of 0.7 ns/m, as compared with 55 ns/m for Ref. 17.

It is interesting to note how the level spacing changes as $A$ increases from 186 to 192. The binding energies for the odd targets ($^{187}$Os and $^{189}$Os) are 7.989 and 7.793 MeV, respectively. The level densities for these two odd targets are quite comparable (30% difference). The binding energies for the even targets ($^{186,188,190,192}$Os) are 6.297, 5.923, 5.760, and 5.589 MeV, respectively. There is a 30% change in $\bar{D}$ from $^{186}$Os to $^{188}$Os corresponding to a 374-keV difference in binding energy. However, there is a difference of nearly a factor of 2 between the $^{188}$Os and $^{190}$Os level densities even though there is only a 160-keV difference in binding energy. One probably can associate this difference with the phase transition from a statically deformed prolate to a $\gamma$-unstable or triaxial shaped nucleus that was observed in giant-resonance studies of the osmium isotopes.[18]

TABLE III. Average level spacings ($D$) for the osmium isotopes.

| Target nucleus | Number of resonances[a] | $\Delta_3$(expt)[b] | $\Delta_3$(theor)[c] | $D$ (eV) Present work | Ref. 16 | Ref. 17 |
|---|---|---|---|---|---|---|
| 186 | 56 | 0.53 | 0.41 ± 0.11 | 30 ± 2 | | 22 ± 6 |
| 187 | 26 | 0.66 | 0.60 ± 0.22 | 4.8 ± 0.2 | 4.42 ± 0.17 | 8 ± 1.6 |
| 188 | 49 | 0.61 | 0.39 ± 0.11 | 40 ± 2 | | 47 ± 10 |
| 189 | 24 | 0.48 | 0.45 ± 0.22 | 3.2 ± 0.2 | 3.33 ± 0.12 | 3.8 ± 0.7 |
| 190 | 17 | 0.39 | 0.28 ± 0.11 | 70 ± 5 | | 52 ± 14 |
| 192 | 18 | 0.42 | 0.30 ± 0.11 | 115 ± 10 | | 140 ± 35 |

[a] This is the number of resonances used to calculate $D$ and $\Delta_3$(expt).

[b] $\Delta_3$(expt) is a measure of the deviation of a straight-line fit to the staircase plots.

[c] $\Delta_3$(theor) is calculated from Eqs. (80) and (81) of Ref. (15) for one-spin and two-spin populations, respectively.

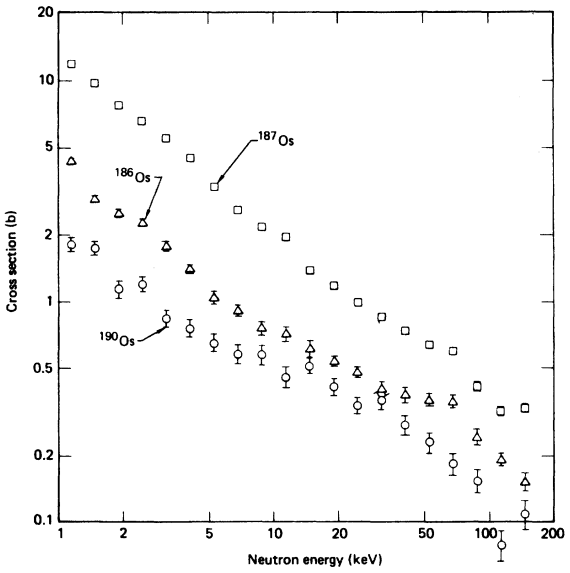


FIG. 7. The average neutron-capture cross sections for $^{186}$Os, $^{187}$Os, and $^{190}$Os. The data are averaged into neutron energy bins of equal lethargy. The data are plotted at the center bin (see text).

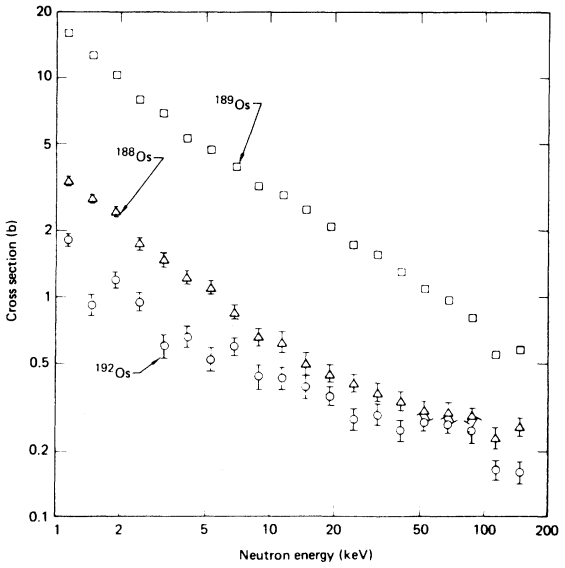


FIG. 8. The average neutron-capture cross sections for $^{188}$Os, $^{189}$Os, and $^{192}$Os. See the caption to Fig. 7.

### B. Average capture cross sections

The data above 1 keV were averaged into neutron-energy bins of equal lethargy, i.e., the ratio of the upper limit $E_u$ to the lower limit $E_l$ for the energy of each bin is given by

$$\ln(E_u/E_l)=0.25.$$

Figures 7 and 8 show the average cross sections from 1 to 150 keV for all of the osmium isotopes measured in the present experiment. Table IV lists these cross-section values and their sta-

TABLE IV. Average capture cross sections for the osmium isotopes.[a]

| $E$ | $\Delta E$[b] | $^{186}$Os | | $^{187}$Os | | $^{188}$Os | | $^{189}$Os | | $^{190}$Os | | $^{192}$Os | |
|---|---|---|---|---|---|---|---|---|---|---|---|---|---|
| (keV) | (keV) | $\sigma$ | $\Delta\sigma$[c] | $\sigma$ | $\Delta\sigma$[c] | $\sigma$ | $\Delta\sigma$[c] | $\sigma$ | $\Delta\sigma$[c] | $\sigma$ | $\Delta\sigma$[c] | $\sigma$ | $\Delta\sigma$[c] |
| 1.145 | 0.145 | 4.33 | 0.125 | 11.86 | 0.160 | 3.38 | 0.156 | 16.15 | 0.192 | 1.80 | 0.128 | 1.81 | 0.121 |
| 1.48 | 0.190 | 2.89 | 0.103 | 9.80 | 0.133 | 2.77 | 0.112 | 12.66 | 0.156 | 1.74 | 0.112 | 0.920 | 0.102 |
| 1.91 | 0.240 | 2.52 | 0.100 | 7.69 | 0.115 | 2.43 | 0.118 | 10.30 | 0.133 | 1.13 | 0.100 | 1.20 | 0.096 |
| 2.465 | 0.315 | 2.28 | 0.084 | 6.58 | 0.106 | 1.73 | 0.106 | 7.76 | 0.113 | 1.20 | 0.093 | 0.945 | 0.091 |
| 3.185 | 0.405 | 1.78 | 0.074 | 5.49 | 0.083 | 1.47 | 0.101 | 6.78 | 0.092 | 0.840 | 0.076 | 0.601 | 0.073 |
| 4.115 | 0.525 | 1.41 | 0.064 | 4.44 | 0.074 | 1.22 | 0.079 | 5.24 | 0.078 | 0.758 | 0.068 | 0.658 | 0.067 |
| 5.32 | 0.680 | 1.05 | 0.062 | 3.30 | 0.063 | 1.09 | 0.073 | 4.69 | 0.071 | 0.657 | 0.062 | 0.517 | 0.062 |
| 6.875 | 0.875 | 0.912 | 0.051 | 2.58 | 0.054 | 0.852 | 0.060 | 3.92 | 0.062 | 0.583 | 0.055 | 0.589 | 0.056 |
| 8.875 | 1.125 | 0.760 | 0.049 | 2.18 | 0.052 | 0.654 | 0.059 | 3.21 | 0.058 | 0.571 | 0.054 | 0.436 | 0.055 |
| 11.45 | 1.45 | 0.711 | 0.050 | 1.95 | 0.048 | 0.618 | 0.064 | 2.92 | 0.054 | 0.455 | 0.050 | 0.430 | 0.051 |
| 14.8 | 1.90 | 0.615 | 0.043 | 1.38 | 0.041 | 0.501 | 0.060 | 2.48 | 0.048 | 0.513 | 0.045 | 0.395 | 0.046 |
| 19.1 | 2.40 | 0.540 | 0.031 | 1.18 | 0.031 | 0.449 | 0.040 | 2.07 | 0.037 | 0.411 | 0.034 | 0.355 | 0.035 |
| 24.65 | 3.15 | 0.476 | 0.028 | 0.992 | 0.027 | 0.406 | 0.036 | 1.72 | 0.031 | 0.336 | 0.029 | 0.280 | 0.030 |
| 31.85 | 4.05 | 0.405 | 0.030 | 0.852 | 0.028 | 0.366 | 0.035 | 1.56 | 0.032 | 0.358 | 0.031 | 0.291 | 0.032 |
| 41.15 | 5.25 | 0.380 | 0.027 | 0.738 | 0.024 | 0.336 | 0.034 | 1.30 | 0.027 | 0.277 | 0.027 | 0.247 | 0.028 |
| 53.2 | 6.80 | 0.360 | 0.022 | 0.639 | 0.019 | 0.304 | 0.029 | 1.09 | 0.021 | 0.229 | 0.022 | 0.270 | 0.022 |
| 68.75 | 8.75 | 0.352 | 0.023 | 0.598 | 0.018 | 0.299 | 0.030 | 0.970 | 0.019 | 0.184 | 0.020 | 0.260 | 0.020 |
| 88.75 | 11.25 | 0.243 | 0.018 | 0.412 | 0.017 | 0.246 | 0.033 | 0.798 | 0.019 | 0.152 | 0.020 | 0.290 | 0.021 |
| 114.5 | 14.5 | 0.193 | 0.012 | 0.320 | 0.013 | 0.227 | 0.025 | 0.543 | 0.014 | 0.075 | 0.015 | 0.165 | 0.016 |
| 148.0 | 19.0 | 0.153 | 0.014 | 0.330 | 0.014 | 0.255 | 0.022 | 0.568 | 0.015 | 0.108 | 0.017 | 0.160 | 0.017 |

[a] All capture cross sections are in barns.
[b] $\Delta E$ is the half-width of the energy bin.
[c] $\Delta\sigma$ is the statistical uncertainty (in barns) only. For systematic uncertainties, see text.

TABLE V. Comparison of $^{186,187,188}$Os$(n,\gamma)$ cross sections from this work with the results of Ref. 4.

| | $^{186}$Os | | $^{187}$Os | | $^{188}$Os | |
|---|---|---|---|---|---|---|
| $E_n$(keV) | Present results | Ref. 4[a] | Present results | Ref. 4[a] | Present results | Ref. 4[a] |
| 5 | 1.15 ± 0.06 | 1.27 | 3.60 ± 0.06 | 3.54 | 1.12 ± 0.07 | 1.23 |
| 10 | 0.74 ± 0.05 | 0.83 | 2.08 ± 0.05 | 2.06 | 0.64 ± 0.06 | 0.71 |
| 20 | 0.53 ± 0.03 | 0.52 | 1.15 ± 0.03 | 1.14 | 0.44 ± 0.04 | 0.45 |
| 30 | 0.42 ± 0.03 | 0.41 | 0.89 ± 0.03 | 0.82 | 0.38 ± 0.03 | 0.37 |
| 50 | 0.37 ± 0.02 | 0.33 | 0.67 ± 0.02 | 0.63 | 0.31 ± 0.03 | 0.31 |
| 100 | 0.22 ± 0.02 | 0.27 | 0.37 ± 0.02 | 0.39 | 0.24 ± 0.03 | 0.25 |
| 150 | 0.15 ± 0.01 | 0.20 | 0.33 ± 0.02 | 0.25 | 0.26 ± 0.02 | 0.26 |

[a]Reference 4 quotes <2% uncertainty in these numbers.

tistical uncertainties.

The results in Table IV for the enriched isotopes were recombined according to their percent abundance in natural osmium (Table I) to construct a $^{nat}$Os capture cross section. The recombined result for $E_n = 31.85 \pm 4.05$ keV is $534 \pm 17$ mb while the measured cross section for the natural osmium sample in the same energy interval is $490 \pm 40$ mb. Although this agreement provides a self-consistency check for our measurement, the result disagrees significantly with a previous measurement at $E_n = 30 \pm 7$ keV by Macklin, Gibbons, and Inada[19] which yielded a value of $300 \pm 30$ mb for the capture cross section of a natural osmium sample.

Table V compares the present results for $^{186,187,188}$Os with those of Winters *et al.*[4] at selected energies between 5 and 150 keV. The agreement between the two measurements is quite good except at the lowest energies where differences in the resonance self-shielding correction might exist.

Reference 3 reported a value of $0.41 \pm 0.04$ for the ratio of the average capture cross sections for $^{186}$Os and $^{187}$Os in the neutron energy interval $25 \pm 2$ keV. These data were obtained using a 25-keV iron-filtered reactor beam. The above result was an average of six measurements that varied from 0.35 to 0.49. The large dispersion in these data was the result of a low signal-to-background ratio which was sensitive to experimental conditions in nearby reactor ports. A reanalysis[20] was recently conducted for one of the six experimental runs in which all of the nearby reactor ports were closed, thereby reducing the background considerably. This reanalysis included extraction of the $^{186}$Os and $^{187}$Os capture cross sections relative to a $^{165}$Ho standard. The result of the reanalysis of this one low background run is $\sigma_c(186) = 452 \pm 70$ mb and $\sigma_c(187) = 953 \pm 135$ mb for $E_n = 25 \pm 2$ keV. These values agree well with the present results of $476 \pm 28$ mb and $992 \pm 27$ mb at $E_n = 24.65 \pm 3.15$ keV for $^{186}$Os and $^{187}$Os, respectively.

Table VI compares the present results for $^{190}$Os and $^{192}$Os with the only other previous measurements; these all were made at 24 keV neutron energy using the neutron-activation technique. For $^{190}$Os, the best agreement is found with the recent results of Bradley *et al.*[21]; for $^{192}$Os, the best agreement is found with the results of Sidappa *et al.*,[22] while there is significant disagreement with those of Bradley *et al.*[21]

### C. Maxwellian-averaged cross sections

For most current models of *s*-process nucleosynthesis, the temperature of the *s*-process site is believed to be on the order of 30 keV. For use in astrophysical applications and in particular for purposes of the Os-Re chronometer described in Sec. V, we averaged our cross-section results for the osmium isotopes using a Maxwell-Boltzmann velocity distribution. The averaged cross section $\bar{\sigma}$ was computed as $\bar{\sigma} = \langle \sigma \cdot v \rangle / v_T$, where the brackets represent the Maxwellian average and $v_T$ is the most probable velocity for the temperature $kT$ of the Maxwellian distribution.

The Maxwellian-averaged cross sections for all the osmium isotopes for a temperature $kT = 30$ keV are listed in Table VII. For the Os-Re chronometer it is the ratio of these results from $^{186}$Os and $^{187}$Os that is of importance. From Table VII, this ratio $\bar{\sigma}(186)/\bar{\sigma}(187)$ is seen to be $0.48 \pm 0.04$. This value is only slightly dependent upon

TABLE VI. Comparison of $^{190,192}$Os$(n,\gamma)$ results at 24 keV neutron energy.[a]

| Reference | $^{190}$Os | $^{192}$Os |
|---|---|---|
| Present work[b] | 336 ± 29 | 280 ± 30 |
| Ref. 21 | 359 ± 38 | 156 ± 16 |
| Ref. 22 | | 296 ± 37 |
| Ref. 23 | 477 ± 71 | |
| Ref. 24 | 886 ± 130 | |

[a]All values in mb.

[b]Present results are for $E_n = 24.65 \pm 3.15$ keV.

TABLE VII. Maxwellian-averaged capture cross sections for the osmium isotopes assuming $kT = 30$ keV. The errors include both statistical and systematic uncertainties.

| Isotope | $\bar{\sigma} = \langle \sigma \cdot v \rangle / v_T$ [a] |
|---|---|
| 186 | 0.438 ± 0.030 |
| 187 | 0.919 ± 0.043 |
| 188 | 0.395 ± 0.024 |
| 189 | 1.536 ± 0.046 |
| 190 | 0.295 ± 0.045 |
| 192 | 0.311 ± 0.045 |

[a] Cross section in barns.

a choice of $kT$ near 30 keV, i.e., there are $<10\%$ variations between 20 and 40 keV. The cosmological implications of this result are noted below.

## V. ASTROPHYSICAL AND COSMOLOGICAL IMPLICATIONS

### A. The age of the elements

The basic mechanisms for the formation of the elements have been delineated in the classic paper of Burbidge *et al.*[25] The elements heavier than iron (where the binding energy per nucleon reaches its maximum) are formed by successive neutron capture, which can proceed on either a slow time scale (the $s$-process) or a rapid one (the $r$-process). The source of neutrons has not been determined unambiguously, but it is thought that the $^{22}Ne(\alpha, n)$ reaction plays the most important role.[26-28] The $s$-process proceeds along the line of $\beta$ stability, terminating at bismuth, and takes place primarily in helium-burning stars; the $r$-process departs substantially from the locus of stable nuclei, is exclusively responsible for production of the elements heavier than bismuth, and takes place primarily in supernovae.

The most important nuclear dating method that is based upon the $r$-process is the U-Th technique of Fowler and Hoyle.[29] This method consists in calculating the production ratios for $^{232}Th$, $^{235}U$, and $^{238}U$ in supernova events, and by measuring the current abundance ratios of the same nuclei, arriving at a chronology of supernova events; and thus, with the use of a model of the time dependence of such events (the same exponential model as is used here), the age of the galaxy. There are two important uncertainties connected with this method (other than the model for supernova frequency employed), namely (1) that the half-lives of the chronometer nuclei are comparable to (and not much longer than) their age and (2) that the calculation of the production ratios of the chronometer nuclei depends heavily upon the (hard-to-test) assumption of equal abundances (production rates) for each of their progenitors. It was Clayton's assertion,[1] therefore, that a nuclear chronometer based upon the $s$-process in general, which would not depend upon the assumption (2), would be more reliable; and that the $^{187}Re \rightarrow {}^{187}Os$ chronometer, in particular, because of the very long half-life of $^{187}Re$, would be best.

An $s$-process chronometer, on the other hand, depends upon the "local" assumption, namely that the product $N\sigma$ is constant for adjacent $s$-process nuclei, where $N$ is the $s$-process abundance for a given nuclear species and $\sigma$ is its Maxwellian-averaged neutron-capture cross section at the temperature appropriate to the stellar site of the $s$-process ($kT \simeq 30$ keV). However, this assumption has been well justified by the work of Macklin *et al.*[30] for the strontium, zirconium, tin, and samarium isotopes; it probably holds even more rigorously for the osmium isotopes, which are far from any nuclear shell closure. Hence, little uncertainty should result from the use of the local assumption.

Figure 9 shows the portion of the chart of the nuclides in the vicinity of the osmium and rhenium isotopes. Both the $s$-process and $r$-process paths are shown. It can be seen that $^{187}Re$ is an $r$-process nucleus and that both $^{186}Os$ and $^{187}Os$ are shielded from the $r$-process, so that the synthesis of $^{186}Os$ and $^{187}Os$ initially involves only the $s$-process. If we denote the $s$-process abundances of $^{186}Os$ and $^{187}Os$ as $N_s^{186}$ and $N_s^{187}$ and the radiogenic component of $^{187}Os$ resulting from the $\beta$ decay of $^{187}Re$ as $N_{\text{rad}}^{187}$, then the total abundances can be written as

$$N^{186} = N_s^{186} \quad \text{and} \quad N^{187} = N_s^{187} + N_{\text{rad}}^{187}. \tag{1}$$

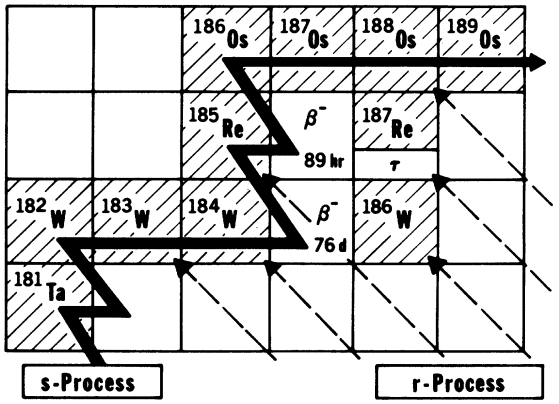


FIG. 9. The $s$-process (heavy line) and $r$-process (dashed lines) in the vicinity of the osmium isotopes. It can be seen that $^{186}Os$ and $^{187}Os$ are shielded from the $r$-process by $^{186}W$ and $^{187}Re$, respectively.

Using the local assumption and Eqs. (1), we can express the ratio of $N_{\text{rad}}^{187}$ to its parent $^{187}$Re abundance $N_{\text{rad}}^{187}$ as

$$R=\frac{N_{\text{rad}}^{187}}{N_{\text{Re}}^{187}}=\frac{N^{187}/N_{\text{Os}}-f(\bar{\sigma}_{186}/\bar{\sigma}_{187})_{\text{lab}}\,(N^{186}/N_{\text{Os}})}{N_{\text{Re}}^{187}/N_{\text{Re}}}\,\frac{N_{\text{Os}}}{N_{\text{Re}}}\,, \tag{2}$$

where $N_{\text{Os}}$ and $N_{\text{Re}}$ are the elemental abundances of osmium and rhenium. The measured Maxwellian-averaged laboratory cross-section ratio $(\bar{\sigma}_{186}/\bar{\sigma}_{187})_{\text{lab}}$ is multiplied by the correction factor $f$ in order to account for the fact that the osmium nuclei in a stellar environment exist in excited states as well as in their ground state. In particular, the 9.8-keV excited state of $^{187}$Os plays an important role here (although no other excited states do, either in $^{186}$Os or in $^{187}$Os at temperatures in the neighborhood of $kT=30$ keV). The most probable value for this factor has been calculated by Woosley and Fowler[6] to be $f=0.83$; it should be noted, however, that somewhat larger values for $f$ (up to ~1.0) are not excluded.[6] The values used for the other parameters in Eq. (2) are listed in Table VIII. The only entry in the table whose uncertainty is significant is that for $N_{\text{Os}}/N_{\text{Re}}$, for which we have chosen to use the value of $13.1\pm0.6$ recommended by Woosley[31]; this value is obtained from elemental analysis of type-$C1$ carbonaceous chondrites only, and excludes the (slightly lower) values from other types of meteorites[32] that are thought to be less ancient. Thus, using the values in Table VIII together with $f=0.83^{+0.07}_{-0}$ and our present result of $(\bar{\sigma}_{186}/\bar{\sigma}_{187})_{\text{lab}}=0.48\pm0.04$, Eq. (2) yields $R=0.124^{+0.017}_{-0.026}$.

Clayton[1] used a simple model to determine the above ratio as a function of the time and duration of nucleosynthesis. He assumed that $r$-process nucleosynthesis (which formed $^{187}$Re) began at a time $\Delta$ before the condensation of the solar system and decreased exponentially at a rate $\lambda_A$. Therefore $\lambda_A$ is a measure of the supernova rate in the galaxy. If $\lambda_B$ denotes the $\beta$-decay rate of $^{187}$Re, one can express the ratio $N_{\text{rad}}^{187}/N_{\text{Re}}^{187}$ at the time of solar system condensation, using the Bateman equations for radioactive growth and decay, as

$$\frac{N_{\text{rad}}^{187}}{N_{\text{Re}}^{187}}=\frac{\lambda_A-\lambda_B}{\lambda_A}\exp(\lambda_B\Delta)\,\frac{1-\exp(-\lambda_A\Delta)}{1-\exp[-(\lambda_A-\lambda_B)\Delta]}-1\,. \tag{3}$$

The two extreme cases of this model are (1) sudden synthesis (a single supernova event), for which $\lambda_A\to\infty$ and Eq. (3) becomes $N_{\text{rad}}^{187}/N_{\text{Re}}^{187}\simeq\lambda_B\Delta$, and (2) uniform synthesis (a constant rate of supernova events), for which $\lambda_A\to0$ and Eq. (3) becomes $N_{\text{rad}}^{187}/N_{\text{Re}}^{187}\simeq\lambda_B\Delta/2$.

It should be noted that not only does case (1) result in the minimum value for $\Delta$, but this value also is the *average* value for $\Delta$, irrespective of the rate (or the rate of change) of supernova events, and hence independent of the model used for the time history of the stellar burning process.

If we solve Eq. (3) for $\Delta$ using the mean lifetime for $^{187}$Re of $\lambda_B^{-1}=6.2\times10^{10}$ yr (Refs. 33–35), $\lambda_A^{-1}=0.43\ \Delta$ (Ref. 36), and the above value for $R$, we find that $\Delta=10.8^{+1.4}_{-2.2}\times10^9$ yr. Adding this value to the (well-known) age of the solar system, we find the age of the galaxy $A_G$ (or of the elements) to be $15.5^{+1.4}_{-2.2}\times10^9$ yr. Finally, using recent estimates of 1 to $2\times10^9$ yr for the time for formation of our galaxy,[37] we find the age of the universe $A_U$ to be approximately $17^{+2}_{-3}\times10^9$ yr. Figure 10 demonstrates the sensitivity of $\Delta$ both to the supernova-rate model used and the value of the measured cross-section ratio. Of the three curves shown in Fig. 10, the two extreme curves represent the two limiting cases for Eq. (3) discussed above and the middle curve represents the exponential model suggested by Fowler,[36] which appears to represent a reasonable compromise between the two extremes. Therefore, the experimental values for $(\bar{\sigma}_{186}/\bar{\sigma}_{187})_{\text{lab}}$ are plotted in Fig. 10 along the middle curve; the value from Ref. 4 lies slightly above the present result. The error flags here represent the uncertainties in the cross-section measurements alone; these uncertainties by themselves do not contribute very much to the overall uncertainty in $\Delta$.

It is important to note that this analysis has ignored any uncertainty in the half-life $\tau_{1/2}^{187}$ of $^{187}$Re. For many years there was a large discrepancy between the geochronometric determination of $\tau_{1/2}^{187}$ by Herr and collaborators[33] ($4.3\pm0.5\times10^{10}$ yr) and the $\beta$-decay measurement of $\tau_{1/2}^{187}$ by Brodzinski and Conway[38] ($6.5\pm1.3\times10^{10}$ yr). Drever and Payne[34] repeated the Brodzinski and Conway experiment with an improved technique

TABLE VIII. Values used in Eq. (2) to compute $N_{\text{rad}}^{187}/N_{\text{Re}}^{187}$.[a]

| | |
|---|---|
| $N^{187}/N_{\text{Os}}$ | $0.0125\pm0.006$ |
| $N^{186}/N_{\text{Os}}$ | 0.0159[b] |
| $N_{\text{Re}}^{187}/N_{\text{Re}}$ | 0.65[b] |
| $N_{\text{Os}}/N_{\text{Re}}$ | $13.1\pm0.6$[c] |

[a] These values, obtained from meteoritic abundance data (Ref. 32), are referred to the time of solar system condensation using $\tau_{1/2}=4.3\times10^{10}$ yr.

[b] The geochemical uncertainties for these quantities are negligible.

[c] Reference 31—see text for discussion.

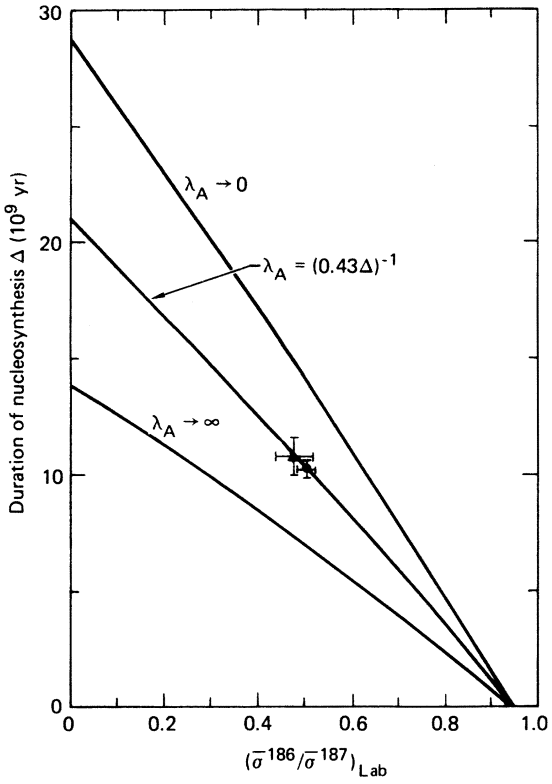


FIG. 10. The duration of nucleosynthesis Δ prior to solar-system condensation as a function of the Maxwellian-averaged laboratory capture cross-section ratio for $^{186}$Os and $^{187}$Os. The three (of the several possible) models for the supernova rate ($\lambda_A$) shown are: uniform ($\lambda_A \to 0$), exponential [$\lambda_A = (0.43\Delta)^{-1}$—Ref. 36], and sudden ($\lambda_A \to \infty$). The present results (triangle) and those of Ref. 4 (circle) are plotted with the uncertainties in the cross-section measurements only.

and obtained $\tau_{1/2}^{187} = 4.7 \pm 0.5 \times 10^{10}$ yr in agreement with the results of Herr *et al.* Unfortunately the Drever and Payne result has never been published. Another, more recent geochronometric determination of $\tau_{1/2}^{187}$ by Luck *et al.*[35] using isotope-dilution mass-spectrometry techniques yielded a result of $4.3 \pm 0.2 \times 10^{10}$ yr, in excellent agreement with the results of Ref. 33. This new result casts doubt upon the data of Ref. 38 and increases our confidence in the above calculation of Δ which includes no uncertainty in the value of $4.3 \times 10^{10}$ yr. If we include all the various measurements, the uncertainty increases in the positive direction. Our best value for the age of the universe then becomes $17 \pm 3 \times 10^9$ yr. Although the new results of Luck *et al.* agree with the previous data of Herr *et al.*, a measurement of $\tau_{1/2}^{187}$ using a different experimental technique would be very valuable. We note in passing that the high temperature and density in a stellar environment also might affect the β-decay half-life significantly.

It should be noted as well that the Hauser-Feshbach calculation of Woosley and Fowler ($f = 0.83$) also predicts the ratio of the inelastic neutron-scattering cross section (to the 9.8-keV state) to the elastic cross section for $^{187}$Os to be about 0.06 at $E_n = 30$ keV. Preliminary results of a recent measurement[39] indicate a smaller value for this ratio, implying a somewhat larger value for the correction factor $f$ than the one used here (for example, a value for $f$ of unity yields $\Delta = 8.6 \times 10^9$ yr if all the other parameters are the same as those used above). However, the final results of this measurement are not yet available, so that we cannot yet predict their ultimate effect upon the value for $f$.

Finally, we note that our value for Δ of $(10.8^{+1.4}_{-2.2}) \times 10^9$ yr is concordant with the value of $(6.1 \pm 2.3) \times 10^9$ yr obtained from the U-Th method of Fowler and Hoyle,[29] but mainly because of the uncertainty associated with the determination of $f$. Thus, a better value for this quantity can help to ascertain the validity of the $r$-process assumption of equal production rates for the progenitors discussed above. Our value for Δ is also in good agreement with the value of $9.5 \times 10^9$ yr for the duration of $s$-process synthesis obtained by Beer and Käppeler[40] using the $s$-process chronometer $^{176}$Lu.

### B. The age of the universe

The age of the universe $A_U$ obtained above from the Re → Os radiogenic determination of the age of the elements is $(17 \pm 3) \times 10^9$ yr. The value of $A_U$ obtained by Iben (Ref. 41, also see Ref. 36) from globular clusters is $(13 \pm 3) \times 10^9$ yr, and that obtained by Sandage and Tammann[42] from the Hubble time $T_H$ is $(16.6 \pm 1.7) \times 10^9$ yr. These values are concordant, but it is clear, since the value for $A_U$ from nuclear cosmochronology is so near to the Hubble time, that if we live in a decelerating universe (corresponding to a null value for the cosmological constant in Einstein's equations), then it is open.

However, there is recent evidence (Ref. 43) that the Hubble time might be substantially smaller than the value given by Sandage and Tammann.[42] If this new value for $T_H \lesssim 10 \times 10^9$ yr were substantiated, the cosmological implications of the combined results of the present experiment and of the work of Ref. 43 are of considerable importance: either Einstein's cosmological constant is not zero, implying a gravitational *repulsion* at large distances, or the hot big-bang theory is itself no longer valid as a description of the past history of the universe.

ACKNOWLEDGMENTS

We would like to acknowledge valuable discussions with Professor R. R. Winters, Professor H. S. Camarda, Professor S. E. Woosley, and Dr. R. L. Macklin. We would like to thank Dr. G. Rogosa for his assistance in obtaining the enriched osmium samples. We also would like to thank the LLL linac operations staff, whose dedication during the long experimental runs was invaluable to the successful completion of this measurement. This work was performed under the auspices of the U.S. Department of Energy by the Lawrence Livermore National Laboratory under Contract No. W-7405-ENG-48.

---

*Present address: Los Alamos Scientific Laboratory, University of California, Los Alamos, New Mexico 87545.

[1]D. D. Clayton, Astrophys. J. 139, 637 (1964).
[2]A preliminary report of this work was published in Nature (London) 262, 197 (1976).
[3]J. C. Browne, G. P. Lamaze, and I. G. Schroder, Phys. Rev. C 14, 1287 (1976).
[4]R. R. Winters, R. L. Macklin, and J. Halperin, Phys. Rev. C 21, 563 (1980).
[5]E. Vogt, in *Advances in Nuclear Physics*, edited by M. Baranger and E. Vogt (Plenum, New York, 1968), Vol. 1, p. 270.
[6]S. E. Woosley and W. A. Fowler, Astrophys. J. 233, 411 (1979).
[7]J. B. Czirr, Nucl. Instrum. Methods 72, 23 (1969).
[8]B. L. Berman and J. C. Browne, Phys. Rev. C 7, 2522 (1973).
[9]G. T. Mattesich, in Cube Symposium Proceedings (CONF-741001, Lawrence Livermore Laboratory, 1974), p. 188.
[10]H. Maier-Leibnitz, Oak Ridge National Laboratory, 1963 (unpublished).
[11]L. Dresner, Nucl. Instrum. Methods 16, 176 (1962).
[12]Evaluated Nuclear Data File, ENDF/B-IV, National Nuclear Cross Section Center, Brookhaven National Laboratory (1976).
[13]H. O. Zetterström, S. Schwarz, and L. G. Strömberg, Nucl. Instrum. Methods 42, 277 (1966).
[14]F. Fröhner and E. Haddad, Nucl. Phys. 71, 129 (1965).
[15]F. J. Dyson and M. L. Mehta, J. Math. Phys. 4, 701 (1963).
[16]A. Stolovy, A. I. Namenson, and B. L. Berman, Phys. Rev. C 14, 965 (1976).
[17]V. P. Vertebnyi, P. N. Vorona, A. I. Kal'chenko, V. A. Pshenichnyi, and V. K. Rudishin, Yad. Fiz. 22, 674 (1975) [Sov. J. Nucl. Phys. 22, 348 (1975)].
[18]B. L. Berman, D. D. Faul, R. A. Alvarez, P. Meyer, and D. L. Olson, Phys. Rev. C 19, 1205 (1979).
[19]R. L. Macklin, J. H. Gibbons, and I. Inada, Phys. Rev. 129, 2695 (1963).
[20]J. C. Browne, G. P. Lamaze, and I. G. Schroder (private communication).
[21]T. Bradley, Z. Parsa, M. L. Stelts, and R. E. Chrien, in *Nuclear Cross Sections for Technology*, edited by J. L. Fowler, C. H. Johnson, and C. D. Bowman, NBS Special Publication No. 594 (NBS, Washington, D. C., 1980), p. 344.
[22]K. Sidappa, M. Sriramachandra Murty, and J. Rama Rao, J. Phys. A 5, 988 (1972).
[23]K. Sidappa, M. Sriramachandra Murty, and J. Rama Rao, Nuovo Cimento 18, 48 (1973).
[24]R. L. Macklin, N. H. Lazar, and W. S. Lyon, Phys. Rev. 107, 504 (1957).
[25]E. M. Burbidge, G. R. Burbidge, W. A. Fowler, and F. Hoyle, Rev. Mod. Phys. 29, 547 (1957).
[26]A. G. W. Cameron, Astron. J. 65, 485 (1960).
[27]B. L. Berman, R. L. Van Hemert, and C. D. Bowman, Phys. Rev. Lett. 23, 386 (1969).
[28]I. Iben, Jr., Astrophys. J. 196, 525 (1975).
[29]W. A. Fowler and F. Hoyle, Ann. Phys. (N.Y.) 10, 280 (1960); W. A. Fowler, in *Proceedings of the R. A. Welch Foundation Conference XXI on Cosmochemistry*, edited by W. O. Milligan (Welch Foundation, Houston, 1978), pp. 90 and 92.
[30]R. L. Macklin, J. H. Gibbons, and T. Inada, Nature (London) 197, 369 (1963); R. L. Macklin, T. Inada, and J. H. Gibbons, *ibid.* 194, 1272 (1962).
[31]S. E. Woosley, private communication.
[32]J. W. Morgan, in *Handbook of Elemental Abundances in Meteorites*, edited by B. Mason (Gordon and Breach, New York, 1972); J. W. Morgan and J. F. Lovering, Geochim. Cosmochim. Acta 31, 1893 (1967).
[33]W. Herr, W. Hoffmeister, B. Hirt, J. Geiss, and F. G. Houtermans, Z. Naturforscher 16a, 1053 (1961); B. Hirt, G. R. Tilton, W. Herr, and W. Hoffmeister, in *Earth Science and Meteorites*, edited by J. Geiss and E. E. Goldberg (North-Holland, Amsterdam, 1963).
[34]R. W. P. Drever and J. A. Payne, as quoted by F. J. Dyson in *Aspects of Quantum Theory*, edited by A. Salam and E. P. Wigner (Cambridge University Press, Cambridge, 1972), p. 225.
[35]J. M. Luck, J. L. Birck, and C. J. Allegre, Nature (London) 283, 256 (1980).
[36]W. A. Fowler, in *Cosmology, Fusion and Other Matters*, edited by F. Reines (Colorado Associated University Press, Boulder, 1972).
[37]V. Trimble, Rev. Mod. Phys. 47, 877 (1975).
[38]R. L. Brodzinski and D. C. Conway, Phys. Rev. 138, B1368 (1965).
[39]R. R. Winters, F. Käppeler, K. Wisshak, B. L. Berman, and J. C. Browne, Bull. Am. Phys. Soc. 24, 854 (1979).
[40]H. Beer and F. Käppeler, Phys. Rev. C 21, 534 (1980).
[41]I. Iben, Jr., Science 155, 785 (1968).
[42]A. Sandage and G. A. Tammann, Astrophys. J. 197, 265 (1975).
[43]M. Aaronson, J. Mould, J. Huchra, W. T. Sullivan, R. A. Schommer, and G. D. Bothun, Astrophys. J. 239, 12 (1980).